Physica B 578 (2020) 411743

Contents lists available at ScienceDirect

Physica B: Physics of Condensed Matter

journal homepage: www.elsevier.com/locate/physb

Two-pulse magnetic field-free switching scheme for perpendicular SOT-MRAM with a symmetric square free layer

R.L. de Orio [a,*], A. Makarov [b], W. Goes [c], J. Ender [a], S. Fiorentini [a], V. Sverdlov [a]

[a] Christian Doppler Laboratory for Nonvolatile Magnetoresistive Memory and Logic at the Institute for Microelectronics, TU Wien, Vienna, Austria
[b] Institute for Microelectronics, TU Wien, Gußhausstraße 27–29/E360, 1040 Vienna, Austria
[c] Silvaco Europe Ltd., Cambridge, United Kingdom

ARTICLE INFO

Keywords:
Spin–Orbit Torque MRAM
Perpendicular magnetization
Magnetic field-free switching
Two-pulse switching scheme

ABSTRACT

A magnetic field-free switching of a symmetric square free layer with perpendicular magnetization by spin–orbit torque is demonstrated based on micromagnetic modeling and numerical simulations. The field-free switching is accomplished by using a two-pulse switching scheme. An appropriate design of the cell structure yields a deterministic and fast switching, about 0.6 ns, of the magnetized free layer. It is shown that the switching is robust with respect to fluctuations of the current pulse duration and, furthermore, very robust in case of delays or overlaps between the writing current pulses.

1. Introduction

Since the invention of the integrated circuit technology the increase in performance and speed of the circuits has been achieved by downscaling the semiconductor devices. This trend, however, is coming to a halt due to increasing dynamic and standby power consumption. Therefore, alternative technologies have to be investigated [1].

Besides charge, the spin is also an inherent property of the electron that can be exploited. Magnetic tunnel junctions (MTJ), formed by two ferromagnetic layers separated by a tunnel barrier, are the key element of magnetoresistive random access memory (MRAM) [2]. Their parallel and anti-parallel arrangements of the magnetization in the ferromagnetic layers and the corresponding low and high resistivity states make this spin-based technology a feasible energy-efficient and non-volatile alternative to charge-based memories. Nevertheless, these emerging memories will only be able to replace the current charge-based counterparts if they can deliver the same level of performance.

Spin-transfer torque MRAM (STT-MRAM) is already available commercially. A critical issue, however, is the increasing current level needed for memory writing with nanosecond timings, which leads to reliability issues [3]. In this context, spin–orbit torque MRAM (SOT-MRAM) appears as a viable solution, as it decouples the reading and writing paths [4]. It combines non-volatility, high speed, and high endurance, and is thus perfectly suited for applications in caches.

However, for a deterministic SOT switching of a perpendicularly magnetized free layer (FL) an external magnetic field still needs to be applied. In order to avoid the additional external field, several field-free schemes have been proposed. Some common solutions are: controlling the shape of the devices [5–7], biasing the FL by employing an exchange coupling to an antiferromagnet (AF) [8–11], and controlling the crystal symmetry during the metal deposition [12,13]. The basic idea of these schemes is to break the mirror symmetry of the system [14]. Nevertheless, these solutions introduce more complexity into the fabrication process and/or are difficult to be downscaled, which hinders the large scale integration of such memory cells.

Recently, more suitable field-free schemes have also been demonstrated based on proper stacking of ferromagnetic layers and heavy metals [15,16]. In this work we demonstrate, based on micromagnetic modeling and numerical simulations, that a magnetic field-free two-pulse switching scheme, previously suggested to accelerate the switching of an in-plane magnetized rectangular FL [4,17], is also suitable for switching of a perpendicularly magnetized symmetric FL of square shape. In this scheme the structure consists of two orthogonal heavy metal wires connected to the magnetic FL. An advantage of this scheme is that its fabrication process is rather simple and compatible with SOT bilayers. The drawback is a larger cell size [18]. Similar to STT-MRAM, the reading is carried out by running the current through the MTJ grown on the FL and determining its tunneling magnetoresistance (TMR).

We demonstrate that an appropriate design of the writing cell leads to a deterministic and fast switching of the perpendicularly magnetized FL of square shape. In contrast to the in-plane shape anisotropy field ensuring the deterministic switching of a rectangular perpendicularly magnetized FL [18], we show that an in-plane magnetic stray field

* Corresponding author.
E-mail address: orio@iue.tuwien.ac.at (R.L. de Orio).

https://doi.org/10.1016/j.physb.2019.411743
Received 31 May 2019; Received in revised form 27 September 2019; Accepted 2 October 2019
Available online 3 October 2019

created by the part of the FL under the partially overlapping second heavy metal wire and acting on the rest of the FL is responsible for the deterministic switching of the symmetric FL of square shape. Moreover, it is shown that the switching scheme is very robust against fluctuations of the current pulse and also against delays or overlaps between the writing current pulses.

2. SOT-Device operation and modeling

The SOT memory cell is shown in Fig. 1. The structure is composed of a perpendicularly magnetized FL on top of a heavy metal wire (NM1) of 3 nm thickness. Another heavy metal wire (NM2), also of 3 nm thickness, lies on top of the FL. The FL dimensions are 25 × 25 × 2 nm^3. While the NM1 wire has a fixed width $w_1 = 25$ nm, NM2 wires of different widths, w_2, have been considered, which means that the NM2 wire can fully or partly cover the FL. The heavy metal wires, NM1 and NM2, are assumed to be of tungsten and the magnetic FL is assumed to be of CoFeB. The set of parameters for this material composition is given in Table 1.

The thermal stability factor of the structure is determined by [2,19]

$$\Delta = \left(K - D\frac{\mu_0 M_S^2}{2} \right) \frac{V}{k_B T}, \tag{1}$$

where K is the anisotropy energy density, D is the demagnetizing coefficient, μ_0 is the vacuum permeability, M_S is the saturation magnetization, V is the volume of the FL, k_B is the Boltzmann constant, and T is the temperature. Here, $D \approx D_z - D_{x(y)}$, where D_z and $D_{x(y)}$ are the demagnetizing factors for rectangular cuboids calculated from the expressions given in [20]. Based on the parameters given in Table 1, a thermal stability factor of about 40 is calculated, thus making the cell suitable for SRAM applications [21].

The writing operation is based on a two-pulse switching scheme, which is illustrated in Fig. 2. First, a pulse of fixed duration $T_1 = 100$ ps and fixed current $I_1 = 200$ μA is applied through the NM1 wire. This results in a current density of 2.7×10^{12} A/m^2. Then, a second consecutive perpendicular pulse with a current magnitude given by $I_2 = (w_2/25\text{ nm})200$ μA is applied through the NM2 wire. This pulse yields the same current density as that of the first pulse. The second current pulse has a variable duration T_2, so the impact of different pulse configurations on the switching dynamics of the FL is investigated. The delay/overlap between the two pulses is determined by the parameter τ, where a negative value corresponds to an overlap and a positive value represents a delay between the pulses, as shown in Fig. 2.

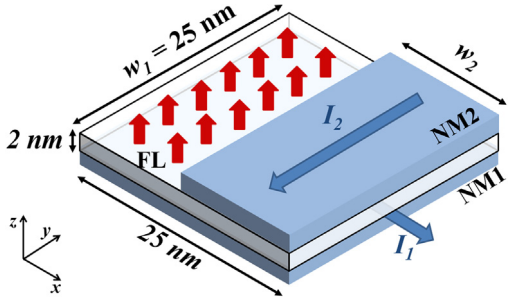

Fig. 1. Two-pulse switching scheme applied to the perpendicularly polarized square magnetic free layer (FL).

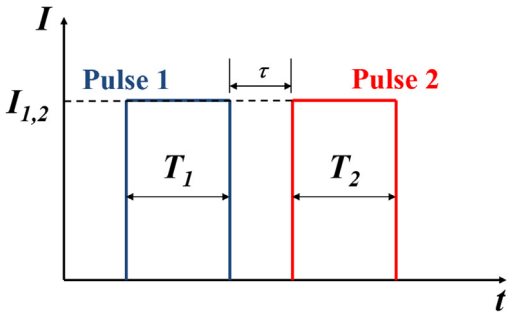

Fig. 2. Square current pulse scheme applied to NM1 and NM2. $T_{1,2}$ is the width of the first/second pulse and τ is the delay/overlap between the pulses. A negative τ represents an overlap, while a positive value represents a delay.

Table 1
Parameters used in the simulations.

Saturation magnetization, M_S	4×10^5 A/m
Exchange constant, A	2×10^{-11} J/m
Perpendicular anisotropy, K	2×10^5 J/m^3
Gilbert damping, α	0.05
Spin Hall angle, θ_{SH}	0.3
Demagnetizing coefficient, D	0.75
Temperature, T	300 K
Free layer dimensions	25 × 25 × 2 nm^3
NM1: $w_1 \times l$	25 × 3 nm^2
NM2: $w_2 \times l$	5 to 25 × 3 nm^2

The magnetization dynamics of the FL is described by the Landau–Lifshitz–Gilbert equation given by [22]

$$\frac{\partial \mathbf{m}}{\partial t} = -\gamma_0 \mathbf{m} \times \mathbf{H_{eff}} + \alpha \mathbf{m} \times \frac{\partial \mathbf{m}}{\partial t} + \frac{1}{M_S}\mathbf{T_S}, \tag{2}$$

where $\mathbf{m}$ is the position-dependent magnetization $\mathbf{M}$ normalized by the saturation magnetization M_S, $\gamma_0 = \mu_0|\gamma|$ is the rescaled gyromagnetic ratio, i.e. the gyromagnetic ratio (γ) rescaled by the vacuum permeability (μ_0), α is the Gilbert damping, and $\mathbf{H_{eff}}$ is an effective magnetic field. This effective field includes various contributions, namely the exchange, uniaxial perpendicular anisotropy, the magnetic field generated by the current pulses, demagnetization, and random thermal field at 300 K [23]. $\mathbf{T_S}$ is the spin–orbit torque caused by the current pulses, which is given by [3]

$$\mathbf{T_S} = +\gamma \frac{\hbar}{2e} \frac{\theta_{SH} I_1}{d w_1 l} \left[\mathbf{m} \times (\mathbf{m} \times \mathbf{y})\right] \Theta(t)\Theta(T_1 - t) \tag{3}$$
$$- \gamma \frac{\hbar}{2e} \frac{\theta_{SH} I_2}{d w_2 l} \left[\mathbf{m} \times (\mathbf{m} \times \mathbf{x})\right] \Theta(t - T_1)\Theta(T_2 + T_1 - t),$$

where e is the elementary charge, $\hbar$ is the Plank constant, θ_{SH} is the effective Hall angle, d is the FL thickness, and l represents the NM thickness.

The magnetization dynamics described by (2) and (3) is solved using a finite difference discretization method implemented in an in-house open-source tool [23]. The values of the parameters used in the simulations are given in Table 1. All numerical simulations are carried out using a mesh size of 2.5 nm×2.5 nm×2.0 nm.

3. Simulation results

Considering, initially, the cell with $w_2 = 25$ nm, where the NM2 wire fully covers the FL, the magnetization dynamics of several realizations are shown in Fig. 3 for a second pulse with $T_2 = 160$ ps. Clearly, the switching is not deterministic as 50% of the realizations do switch (m_z flipped) while the other 50% do not (m_z failed).

The first current pulse (along the $+x$ axis) puts the magnetization in the plane of the FL along the $+y$ direction ($m_y = +1$ and $m_z = 0$ in Fig. 3). Then, the second current pulse (along the $-y$ axis) puts the magnetization of the whole FL along the $-x$ direction ($m_x = -1, m_z = 0$). After the pulse is removed, due to the random thermal field the magnetization relaxes with equal probabilities either to the initial $+z$ direction or to complete the switching towards $-z$ direction. Thus, the switching is not deterministic.

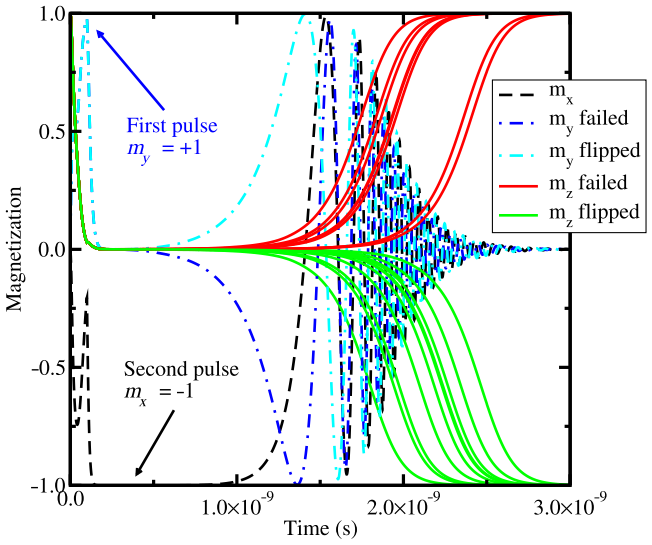

Fig. 3. Magnetization components for several realizations for structures with $w_2 = 25$ nm. $T_1 = 100$ ps, $T_2 = 160$ ps, and $\tau = 0$ ps. The typical magnetization vector components m_x and m_y are also shown.

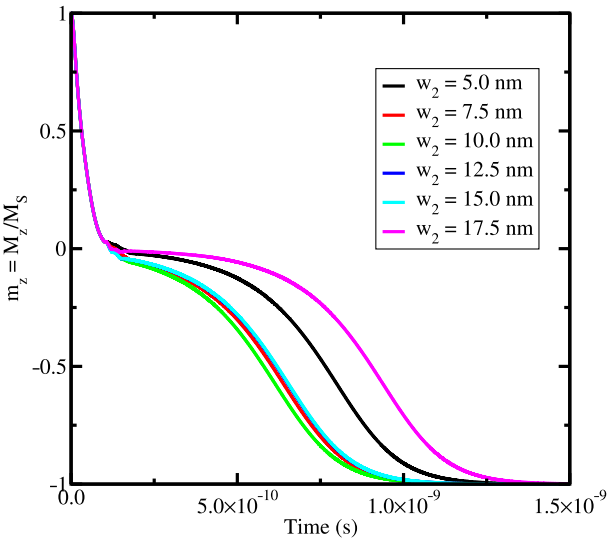

Fig. 4. Magnetization switching for different overlaps between the NM2 wire and the FL. The simulations are carried out for current pulses with $T_1 = 100$ ps, $T_2 = 80$ ps, and $\tau = 0$ ps are used.

Next, NM2 wires with different widths have been tested, where the NM2 wire covers the FL just partially, i.e. $w_2 < 25$ nm. We have found that the partial overlap between the NM2 wire and the FL leads to a deterministic switching. Fig. 4 shows a comparison between the magnetization dynamics for structures with different dimensions of w_2, where each curve represents an average of 20 realizations.

A typical magnetization vector dynamics for $w_2 = 10$ nm is shown in Fig. 5. After the magnetization is placed in the plane of the FL ($m_y = +1, m_z = 0$) by the first current pulse (Fig. 5(a), (b)), the SOT rotates the magnetization under the NM2 wire towards $-x$ due to the second pulse (Fig. 5(c)). In this case the stray field of the FL part under the NM2 wire lies in the plane and has an x-component transverse to

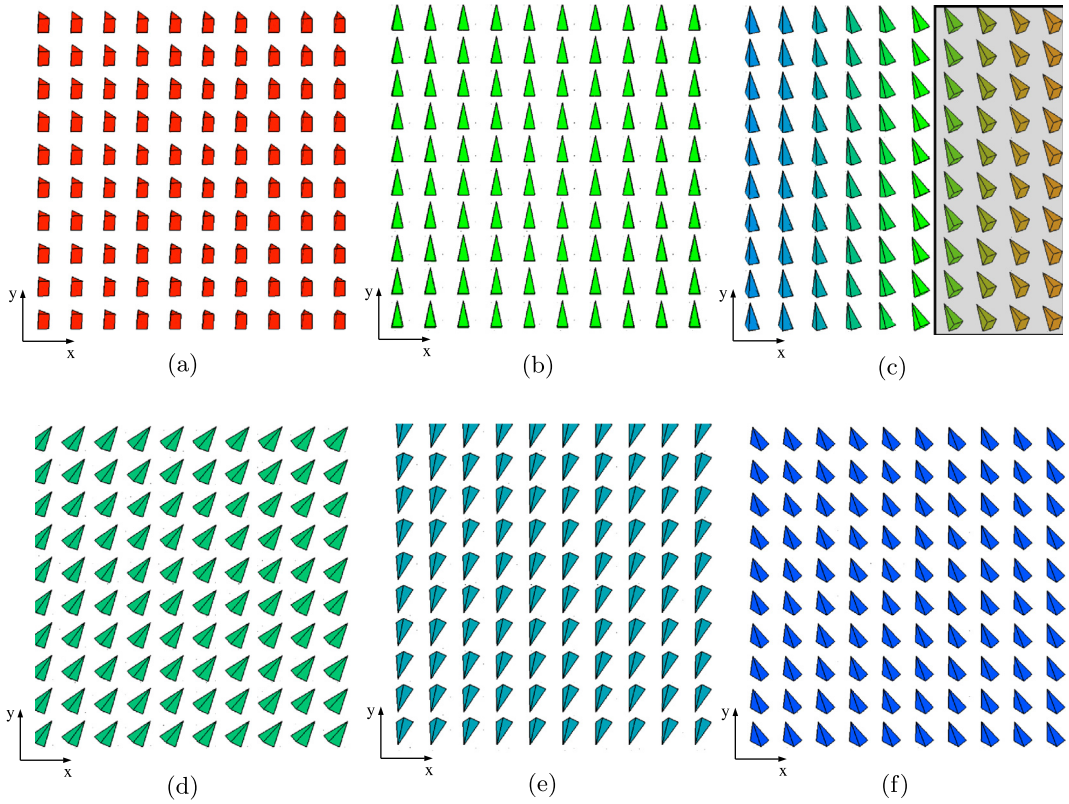

Fig. 5. Snapshots of the magnetization vector during the switching for the cell with $w_2 = 10$ nm, $T_1 = 100$ ps, $T_2 = 80$ ps, and $\tau = 0$ ps. (a) $t = 0$ (first pulse starts), magnetization points to $+z$ (into the plane of the paper). (b) $t = 100$ ps (end of first pulse), magnetization is in $+y$ direction. (c) $t = 180$ ps (just after the end of the second pulse), magnetization under the NM2 wire (highlighted in gray) rotates towards $-x$. (d), (e), and (f) $t = 300$ ps, 400 ps, and 520 ps, respectively, magnetization precesses and switches towards $-z$.

the magnetization of the rest of the FL. As a consequence, this field causes the magnetization of the rest of the FL to precess away from its in-plane orientation. Once this occurs, the magnetization dynamics is uniform and further supported by the perpendicular anisotropy that, ultimately, leads to the deterministic switching (Fig. 5(d), (e), (f)).

The effect of the second pulse duration T_2 on the magnetization switching for $w_2 = 10$ nm is shown in Fig. 6. For a pulse with duration in the range 60 ps $\leq T_2 \leq$ 100 ps the curves nearly coincide. A summary of the switching times as a function of the NM2 wire width and the pulse duration is given in Fig. 7. The shortest switching time (taken at the time when $m_z = -0.5$) is about 0.6 ns, obtained for $w_2 = 10$ nm and $T_2 \leq 100$ ps. The longest switching time, 0.9 ns ($T_2 \leq 100$ ps), is seen for $w_2 = 17.5$ nm, the structure with the largest NM2 wire width for which deterministic switching is observed. It is interesting to note that the switching times are very close to the minimum value for NM2 wire widths in the range 7.5 nm $\leq w_2 \leq$ 15 nm and pulse durations 60 ps $\leq T_2 \leq$ 100 ps.

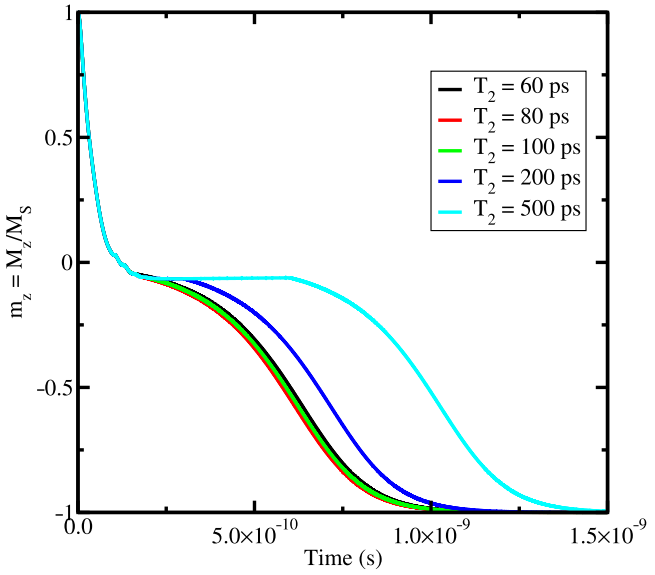

Fig. 6. Average of 20 switching realizations for $w_2 = 10$ nm. Reliable switching is observed for all T_2. The simulations assume $T_1 = 100$ ps and $\tau = 0$ ps.

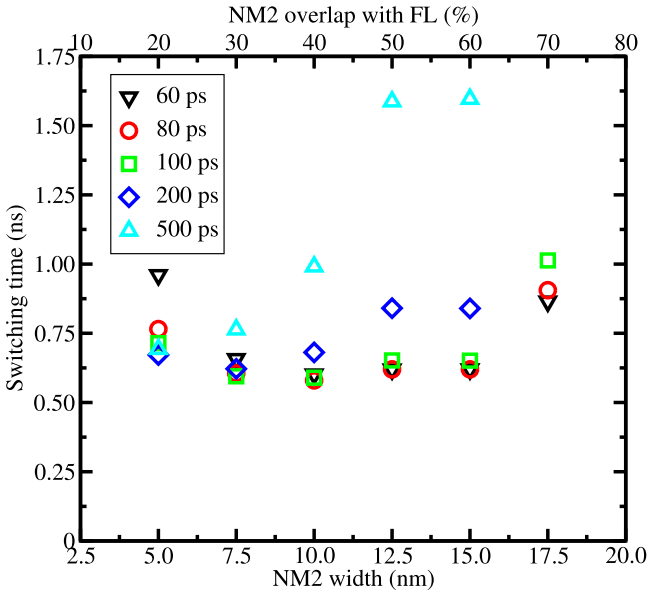

Fig. 7. Summary of switching times as function of the NM2 wire width, w_2, for several current pulse durations, T_2. The simulations consider $T_1 = 100$ ps and $\tau = 0$ ps.

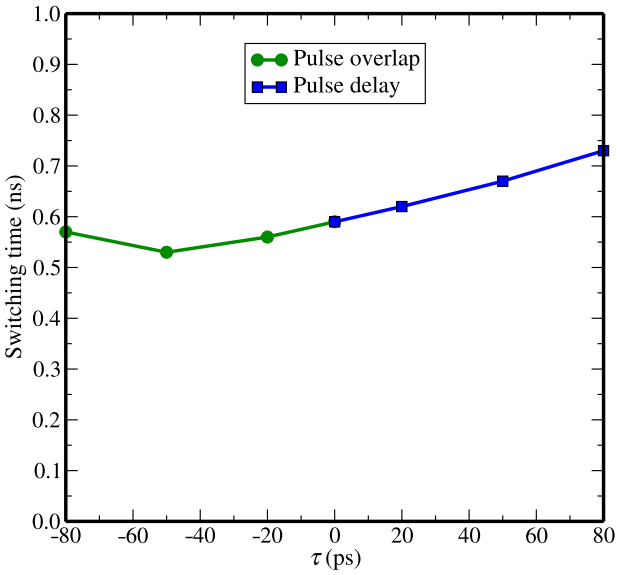

Fig. 8. Switching time as function of the delay/overlap between the first and the second pulse. $\tau < 0$ represents an overlap and $\tau > 0$ indicates a delay between the pulses. The simulations are carried out for a cell with $w_2 = 10$ nm and current pulses with $T_1 = T_2 = 100$ ps.

In the previous simulations $\tau = 0$ (see Fig. 2) was assumed. This represents an ideal situation, when the second current pulse starts exactly when the first pulse ends. Such a perfect synchronization between the pulses is not realistic in practice, and a time delay or an overlap between the pulses is expected to occur as the signals propagate through the interconnect wires. In order to study the cell switching for the more realistic case of delay/overlap between current pulses, we simulated the magnetization dynamics for different values of τ and obtained the switching times. For the cell with $w_2 = 10$ nm and for $T_2 = 100$ ps, the impact of the delay/overlap between the first and second pulses on the switching time is shown in Fig. 8.

It is interesting to note that for short overlaps the switching time is reduced to about 0.5 ns. Moreover, even for large values of delay/overlap the switching time remains in the range 0.5 ns – 0.7 ns. Thus, it can be concluded that the scheme is extremely robust even in the occurrence of relatively long delay/overlap between the pulses.

4. Conclusion

Magnetic field-free switching of a symmetric perpendicularly magnetized free layer of a square shape by SOT is demonstrated by employing two perpendicular consecutive current pulses. A short switching time of 0.6 ns has been obtained. The optimal overlap between the NM2 wire and the FL is found to be between 30%–60%, as the switching remains practically the same at the minimum value. Moreover, the switching scheme is extremely robust, yielding a large confidence window with respect to pulse duration fluctuations and also with respect to delays or overlap between the pulses.

Declaration of competing interest

The authors declare that they have no known competing financial interests or personal relationships that could have appeared to influence the work reported in this paper.

Acknowledgments

This work was supported by the Austrian Federal Ministry for Digital and Economic Affairs and the National Foundation for Research, Technology and Development, Austria.

References

[1] O. Golonzka, J.-G. Alzate, U. Arslan, M. Bohr, P. Bai, J. Brockman, B. Buford, C. Connor, N. Das, B. Doyle, et al., MRAM as embedded non-volatile memory solution for 22FFL FinFET technology, in: Proc. of the 2018 IEDM, 2018, pp. 18.1.1–18.1.4, http://dx.doi.org/10.1109/IEDM.2018.8614620.

[2] D. Apalkov, B. Dieny, J.M. Slaughter, Magnetoresistive random access memory, Proc. IEEE 104 (10) (2016) 1796–1830, http://dx.doi.org/10.1109/JPROC.2016.2590142.

[3] S.-W. Lee, K.-J. Lee, Emerging three-terminal magnetic memory devices, Proc. IEEE 104 (10) (2016) 1831–1843, http://dx.doi.org/10.1109/JPROC.2016.2543782.

[4] V. Sverdlov, A. Makarov, S. Selberherr, Reliable sub-nanosecond switching of a perpendicular SOT-MRAM cell without external magnetic field, J. Syst. Cybern. Inf. 16 (2) (2018) 55–59.

[5] G. Yu, P. Upadhyaya, Y. Fan, J.G. Alzate, W. Jiang, K.L. Wong, S. Takei, S.A. Bender, L.-T. Chang, Y. Jiang, et al., Switching of perpendicular magnetization by spin-orbit torques in the absence of external magnetic fields, Nature Nanotechnol. 9 (2014) 548—554, http://dx.doi.org/10.1038/nnano.2014.94.

[6] G. Yu, L.-T. Chang, M. Akyol, P. Upadhyaya, C. He, X. Li, K.L. Wong, P.K. Amiri, K.L. Wang, Current-driven perpendicular magnetization switching in Ta/CoFeB/[TaOx or MgO/TaOx] films with lateral structural asymmetry, Appl. Phys. Lett. 105 (10) (2014) 102411, http://dx.doi.org/10.1063/1.4895735.

[7] C.K. Safeer, E.J.A. Lopez, L. Buda-Prejbeanu, S. Auffret, S. Pizzini, O. Boulle, I.M. amd G. Gaudin, Spin-orbit torque magnetization switching controlled by geometry, Nature Nanotechnol. 11 (2016) 143—146, http://dx.doi.org/10.1038/nnano.2015.252.

[8] S. Fukami, C. Zhang, S. DuttaGupta, A. Kurenkov, H. Ohno, Magnetization switching by spin-orbit torque in an antiferromagnet-ferromagnet bilayer system, Nature Mater. 15 (2016) 535—541, http://dx.doi.org/10.1038/nmat4566.

[9] A. van den Brink, G. Vermijs, A. Solignac, J. Koo, J.T. Kohlhepp, H.J.M. Swagten, B. Koopmans, Field-free magnetization reversal by spin-hall effect and exchange bias, Nature Commun. 7 (2016) 10854, http://dx.doi.org/10.1038/ncomms10854.

[10] Y.-C. Lau, D. Betto, K. Rode, J.M.D. Coey, P. Stamenov, Spin-orbit torque switching without an external field using interlayer exchange coupling, Nature Nanotechnol. 11 (2016) 758—762, http://dx.doi.org/10.1038/nnano.2016.84.

[11] Y.-W. Oh, S.-H.C. Baek, Y.M. Kim, H.Y. Lee, K.-D. Lee, C.-G. Yang, E.-S. Park, K.-S. Lee, K.-W. Kim, G. Go, J.-R. Jeong, B.-C. Min, H.-W. Lee, K.-J. Lee, B.-G. Park, Field-free switching of perpendicular magnetization through spin-orbit torque in antiferromagnet/ferromagnet/oxide structures, Nature Nanotechnol. 11 (2016) 878—884, http://dx.doi.org/10.1038/nnano.2016.109.

[12] D.S.D. MacNeill, M. Guimaraes, R. Buhrman, J. Park, D. Ralph, Control of spin-orbit torques through crystal symmetry in WTe2/Ferromagnet bilayers, Nat. Phys. 13 (2016) 300—305, http://dx.doi.org/10.1038/nphys3933.

[13] J. Torrejon, F. Garcia-Sanchez, T. Taniguchi, J. Sinha, S. Mitani, J.-V. Kim, M. Hayashi, Current-driven asymmetric magnetization switching in perpendicularly magnetized CoFeB/MgO heterostructures, Phys. Rev. B 91 (2015) 214434, http://dx.doi.org/10.1103/PhysRevB.91.214434.

[14] K.L. Wang, X. Kou, P. Upadhyaya, Y. Fan, Q. Shao, G. Yu, P.K. Amiri, Electric-field control of spin-orbit interaction for low-power spintronics, Proc. IEEE 104 (10) (2016) 1974–2008, http://dx.doi.org/10.1109/JPROC.2016.2573836.

[15] S.-H.C. Baek, V.P. Amin, Y.-W. Oh, G. Go, S.-J. Lee, G.-H. Lee, K.-J. Kim, M.D. Stiles, B.-G. Park, K.-J. Lee, Spin currents and spin-orbit torques in ferromagnetic trilayers, Nature Mater. 17 (2018) 509–513, http://dx.doi.org/10.1038/s41563-018-0041-5.

[16] Q. Ma, Y. Li, D.B. Gopman, Y.P. Kabanov, R.D. Shull, C.L. Chien, Switching a perpendicular ferromagnetic layer by competing spin currents, Phys. Rev. Lett. 120 (2018) 117703, http://dx.doi.org/10.1103/PhysRevLett.120.117703.

[17] S. Fukami, T. Anekawa, C. Zhang, H. Ohno, A spin-orbit torque switching scheme with collinear magnetic easy axis and current configuration, Nature Nanotechnol. 11 (2016) 621—626, http://dx.doi.org/10.1038/nnano.2016.29.

[18] V. Sverdlov, A. Makarov, S. Selberherr, Two-pulse sub-ns switching scheme for advanced spin-orbit torque mram, Solid-State Electron. 155 (2019) 49–56, http://dx.doi.org/10.1016/j.sse.2019.03.010.

[19] K. Watanabe, B. Jinnai, S. Fukami, H. Sato, H. Ohno, Shape anisotropy revisited in single-digit nanometer magnetic tunnel junctions, Nature Commun. 9 (2018) 663, http://dx.doi.org/10.1038/s41467-018-03003-7.

[20] A. Aharoni, Demagnetizing factors for rectangular ferromagnetic prisms, J. Appl. Phys. 83 (6) (1998) 3432–3434, http://dx.doi.org/10.1063/1.367113.

[21] K. Ikegami, H. Noguchi, S. Takaya, C. Kamata, M. Amano, K. Abe, K. Kushida, E. Kitagawa, T. Ochiai, N. Shimomura, et al., MTJ-Based Normally-Off Processors with Thermal Stability Factor Engineered Perpendicular MTJ, L2 Cache Based on 2T-2MTJ Cell, L3 and Last Level Cache Based on 1T-1MTJ Cell and Novel Error Handling Scheme, in: Proc. of the 2015 IEDM, 2015, pp. 25.1.1–25.1.4, http://dx.doi.org/10.1109/IEDM.2015.7409762.

[22] S. Lepadatu, Unified treatment of spin torques using a coupled magnetisation dynamics and three-dimensional spin current solver, Sci. Rep. 7 (2017) 12937, http://dx.doi.org/10.1038/s41598-017-13181-x.

[23] A. Makarov, Modeling of emerging resistive switching based memory cells, Institute for Microelectronics, TU Wien, Vienna, 2014, URL: www.iue.tuwien.ac.at/phd/makarov/.